Very High-Frequency Small-Signal Equivalent Circuit for Short Gate-Length InP HEMT's

Agnès Miras and Eric Legros

***Abstract*— A small-signal equivalent circuit for short gate-length InP high electron-mobility transistors (HEMT's) operating at very high frequency (HF) is proposed. First, the extrinsic parameters of the equivalent circuit are determined using a cold HEMT, but without forward gate bias. Then the intrinsic parameters of the equivalent circuit are extracted, including the frequency dependence of some of them. A fast and accurate method based on least-squares regressions is presented to obtain the extrinsic and intrinsic parameters from measured S-parameters. The improved equivalent circuit accurately fits the S-parameters of 0.25—μm InP HEMT's over the 500-MHz up to 40-GHz measurement bandwidth, for all gate-to-source and drain-to-source voltages.**

***Index Terms*—CAO, equivalent circuit, HEMT, InP, modeling, small-signal.**

I. Introduction

RECENT progress of indium phosphide-based (InP) technology allowed the fabrication of short gate-length InP high electron-mobility transistors (HEMT's) with very high performances. Designing monolithic microwave integrated circuits (MMIC's) requires an accurate knowledge of the electrical characteristics of the transistors. For GaAs–FET's, several models have been established which can be extended to InP HEMT's up to 40 GHz. The models, derived directly from [1], are well suited up to 25 GHz [8], [10]. Improvements have been made on GaAs-FET models [3], [9], [12]–[15], showing the difficulty to simultaneously and accurately fit the four S-parameters over a large frequency range. An InP HEMT model has already been presented [16] up to 60 GHz, but this paper's approach is different and leads to an easy implementation and an accurate model over the large frequency range (500 MHz up to 40 GHz) of the authors' application, for the design of both narrow-band amplifiers tuned to 38 and 40 GHz, and broad-band distributed-amplifiers based on InP HEMT technology.

The presented equivalent circuit is derived from the symmetrical one (at $V_{\rm ds} = 0$) [3] validated for GaAs FET's, and has been extended with respect to the following points.

1) These InP HEMT's are sensitive to forward gate bias. Performing microwave measurements by setting a positive current in the Schottky gate can cause gate failure. Thus, for cold modeling, a measurement at a minimum forward gate-to-source voltage is proposed.
2) Taking into account the frequency dependence of some intrinsic parameters allows the corresponding equivalent circuit to fit the S-parameters with better accuracy. Owing to the systematic study of both real and imaginary parts of intrinsic Y-parameters according to frequency, an improved equivalent circuit has been established (see Fig. 1).
3) A solution method making successive regressions on both the real and imaginary parts of intrinsic Y-parameters allows one to get the values of intrinsic parameters. A powerful advantage of this software is to get analytical forms of Y-, S-, or Z-parameters, with a graphical checking of validity.

The steps to extract the parameters from S-parameters measurements are similar to those described in [1]. In Section II, the extrinsic parameters are first determined using a cold HEMT at $V_{\rm ds} = 0$, $V_{\rm gs} = 0$ and pinchoff voltage. In Section III, the intrinsic parameters are determined by solving the Y-parameters system derived from measured S-parameters by the Y- and Z-parameters' conversions. These transformations allows one to de-embed the extrinsic parameters. The fast solution method based on least-squares regressions automatically calculates the whole set of parameters, and is presented in Section IV. Comparisons showing good agreement between theoretical and experimental S-parameters for typical gate- and drain-to-source voltages are illustrated in Section V, before concluding in Section VI. Some particular points, taken among the above-mentioned papers, will be discussed in the following sections focusing on several approaches of transistor electrical characterization.

II. Determination of Extrinsic Parameters

The determination of extrinsic parameters is performed at $V_{\rm ds} = 0$ (cold HEMT), which allows the equivalent circuit to be simplified.

The parasitic resistances and inductances of the gate, drain, and source are first determined. The method used in [1] consists of forward biasing the gate. But in the case of this paper's InP HEMT's, performing microwave measurements at this forward bias requires a positive current (of several mA) in the gate Schottky diode, and can induce irreversible damages (depending on traps under the gate). It is difficult to find a strong enough forward gate bias to make the method of [1] work. Experimentally, such a compromise is not found concerning the authors' InP HEMT's, which are less forward gate bias-resistant than GaAs ones. Moreover, the removal of a critical gate bias tuning allows an easier implementation of the automatic extraction on wafer.

Manuscript received December 24, 1995; revised March 24, 1997.

The authors are with France Télécom-CNET/PAB, Laboratoire de Bagneux, F-92225 Bagneux Cedex, France.

Publisher Item Identifier S 0018-9480(97)04450-5.

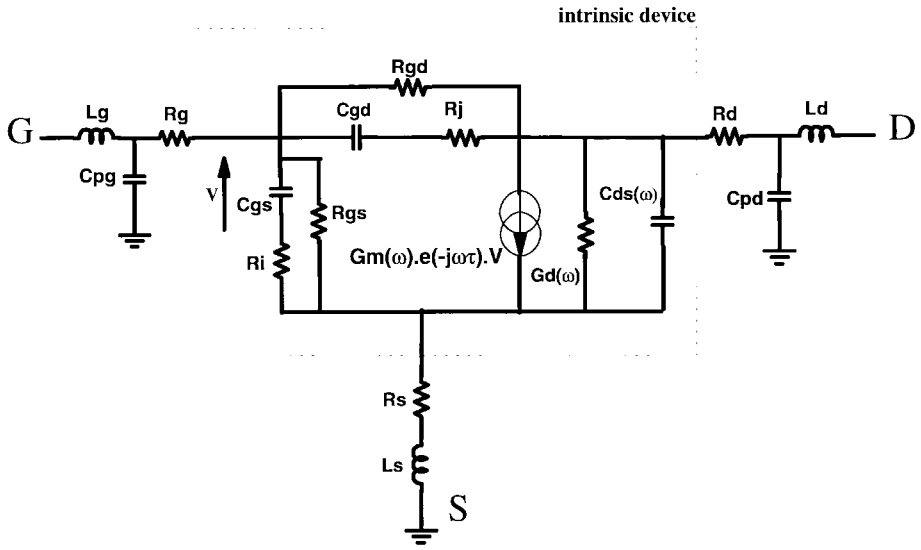

Fig. 1. Small-signal equivalent circuit of InP HEMT's up to 40 GHz including the intrinsic parameters dependence with frequency: $C_{\rm ds}(\omega)$, $G_d(\omega)$, and $G_m(\omega)$.

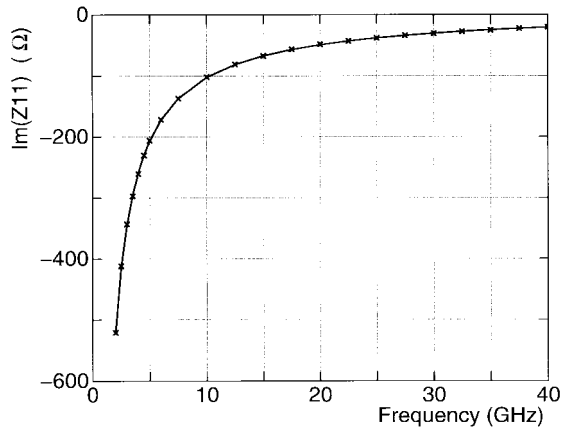

Fig. 2. Imaginary part of Z_{11}-parameter versus frequency described by (3a) for the cold HEMT at $V_{\rm gs} = 0$ V/$V_{\rm ds} = 0$ V, yielding $L_s + L_g = 22.6$ pH and $C_{\rm gch} = 154$ fF (0.25×100 μm^{2}InP HEMT).

A cold HEMT was measured at a minimum forward gate-to-source voltage (high enough for effective conduction in the channel). In fact, $V_{\rm gs}$ will be 0 Vfor a depletion HEMT (normally on), and a few hundred millivolts above the pinchoff voltage for an enhancement HEMT (normally off).

As $V_{\rm gs}$ is taken as low as possible (before reaching a strong forward gate conduction), the modeling of Z_{11} requires taking into account the contribution of the parasitic capacitance $C_{\rm gch}$ under the gate, in parallel with the Schottky dynamic resistance $R_{\rm gch}$ [1]. Then at $V_{\rm ds} = 0$ V, the equivalent impedance of the gate junction can be simplified as follows:

$$Z_{\rm gch} = \frac{R_{\rm gch}}{1 + j\omega \cdot C_{\rm gch} \cdot R_{\rm gch}}. \tag{1}$$

For any gate bias condition, the intrinsic impedance parameters z_{ij} of the equivalent circuit are deduced [1] as follows:

$$\begin{aligned} z_{11} &= R_{\rm ch}/3 + Z_{\rm gch} \\ z_{12} &= z_{21} = R_{\rm ch}/2 \\ z_{22} &= R_{\rm ch} \end{aligned} \tag{2}$$

where $R_{\rm ch}$ is the channel resistance; the constant factors 1/3 and 1/2 take into account the distributed *RC* network under the gate (represented here by the lumped elements $R_{\rm gch}$, $C_{\rm gch}$, and $R_{\rm ch}$).

Since this paper's InP HEMT's gate is not driven at a large enough forward bias, $Z_{\rm gch}$ cannot be simplified to $R_{\rm gch}$ as can a GaAs FET. Thus, since the influence of $C_{\rm pd}$ and $C_{\rm ds}$ is negligible, and $C_{\rm pg}$ is mainly included in $C_{\rm gch}$, the extrinsic Z-parameters are obtained by adding both extrinsic access resistances and inductances as follows:

$$\begin{aligned} Z_{11} = R_s + R_g + \frac{R_{\rm ch}}{3} + \frac{R_{\rm gch}}{1 + (R_{\rm gch} \cdot C_{\rm gch} \cdot \omega)^2} \\ + j\omega \cdot \left[L_s + L_g - \frac{R_{\rm gch}^2 \cdot C_{\rm gch}}{1 + (R_{\rm gch} \cdot C_{\rm gch} \cdot \omega)^2} \right] \end{aligned} \tag{3a}$$

$$Z_{12} = Z_{21} = R_s + \frac{R_{\rm ch}}{2} + j\omega \cdot L_s \tag{3b}$$

$$Z_{22} = R_s + R_d + R_{\rm ch} + j\omega \cdot (L_s + L_d). \tag{3c}$$

The theoretical equations of Z_{ij} are in very good agreement with measurements up to 40 GHz.

To determine the three parasitic inductances L_g, L_d, and L_s, $\mathrm{Im}(Z_{12})$ and $\mathrm{Im}(Z_{22})$ are fitted by standard linear regressions. $\mathrm{Im}(Z_{11})$ is fitted by the function of ω defined as $g_1(\omega) = a \cdot \omega + b \cdot \omega/(1 + c \cdot \omega^2)$, to obtain L_g and $C_{\rm gch}$. The extraction procedure of coefficients is detailed in Section IV.

The frequency response of $\mathrm{Im}(Z_{11})$ is shown in Fig. 2. Equation (3a) shows that the imaginary term $\mathrm{Im}(Z_{11})$ includes $L_s + L_g$ and a corrective term, which can be reduced to $-1/(C_{\rm gch} \cdot \omega)$; this is due to the high value of $R_{\rm gch}$ (several kΩ) compared to $1/(C_{\rm gch} \cdot \omega)$ when the gate Schottky diode is at the onset of forward biasing. Two consequences are induced by this approximation. First, because the imaginary corrective term becomes large for low values of the angular frequency ω, the function $g_1(\omega)$ has to be fitted from typically 2 GHz up to 40 GHz, to avoid fitting at least-squares on a high negative part of $\mathrm{Im}(Z_{11})$. In addition, the sum $L_s + L_g$ and the $C_{\rm gch}$

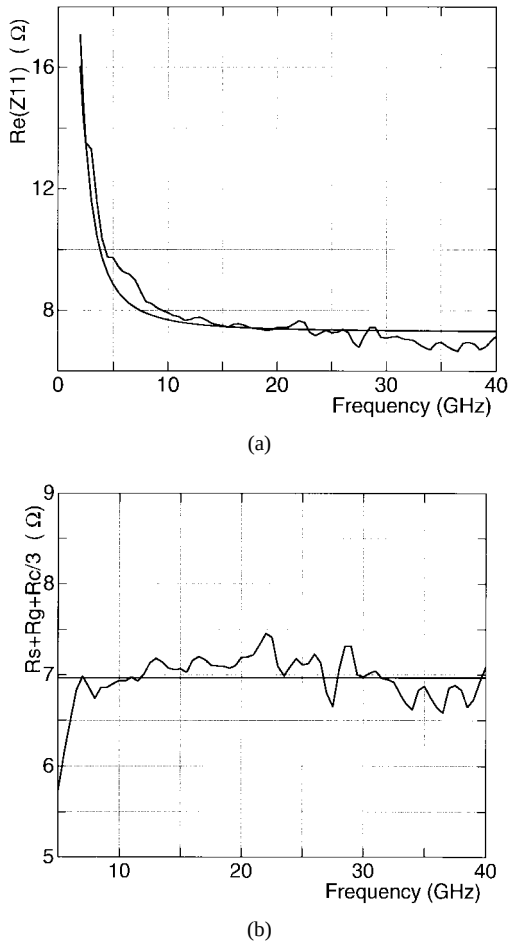

Fig. 3. (a) Real part of Z_{11}-parameter versus frequency for the cold HEMT at $V_{\rm gs} = 0$ V/$V_{\rm ds} = 0$ V ($0.25 \times 100\ \mu$m^{2}InP HEMT). (b) Graph presenting $R_s + R_g + R_{\rm ch}/3$ described by (3a), yielding $R_s + R_g + R_{\rm ch}/3 = 7\Omega$ and $R_{\rm gch} = 10.9$ kΩ.

capacitance value (a few hundreds of femtofarad) are extracted with very good accuracy.

To determine the three parasitic resistances R_g, R_d, and R_s, $\mathrm{Re}(Z_{12})$ and $\mathrm{Re}(Z_{22})$ are fitted by standard linear regressions. An accurate fit of $\mathrm{Re}(Z_{11})$ needs to accurately determine the $R_{\rm gch}$ resistance. However, the real corrective term $R_{\rm gch}/(1+(R_{\rm gch}\cdot C_{\rm gch}\cdot\omega)^2)$ tends to approximately $1/(R_{\rm gch}\cdot C_{\rm gch}^2\cdot\omega^2)$ for $R_{\rm gch}\cdot C_{\rm gch}\cdot\omega \gg 1$. So, the very high value of $R_{\rm gch}$ cannot be easily determined because of the strong decrease of $\mathrm{Re}(Z_{11})$ according to ω, as is shown in Fig. 3(a). Then the extraction procedure consists in fitting $\mathrm{Re}(Z_{11})$ by the function $g_2(\omega) = a + b/\omega^2$, to get an approximate value of $R_{\rm gch}$, which is used as an initial value for the following iterative calculations. For different $R_{\rm gch}$ values chosen by an appropriate algorithm, the expression $\mathrm{Re}(Z_{11}) - R_{\rm gch}/(1+(R_{\rm gch}\cdot C_{\rm gch}\cdot\omega)^2)$ is calculated until it becomes constant, which finally gives the value of $R_s + R_g + R_{\rm ch}/3$, as shown in Fig. 3(b). This sum is then determined accurately.

For very low values of R_g (a few hundreds of milliohms), static determination is preferred. R_g is then determined by measuring from pad to pad the resistance of a purposely designed gate.

At this stage, an additional relation between the parasitic resistances (R_s, R_d, R_g, and $R_{\rm ch}$) is needed. Different methods exist [4], [5] to provide the required additional static relation; in this case, the resistance of the channel under the gate $R_{\rm ch}$ is calculated by

$$R_{\rm ch} = R_{sq} \cdot \frac{L_g}{W_g} \tag{4}$$

where R_{sq} is the sheet resistance of the channel measured by the well-known transmission-line matrix (TLM) method. The TLM method consists of successively measuring the resistance of the layer of interest between several pads with different spacings. A linear variation of the resistance with pad spacing is deduced. R_{sq} is the slope of the linear function. The TLM method is used to de-embed the drain and source contact resistance from the resistance of the layer.

An accurate value of R_{sq} for the HEMT channel should result from TLM's with gates of different lengths. But in this case, the experimental TLM's measurements give a bad accuracy. The main cause comes from the differences between the technological parameters involved in the gate recess etching of different gate lengths. The authors' TLM method does not take into account the recess-etched gate, which implies an underestimation of the R_{sq} value. A simpler approximation could then be to neglect $R_{\rm ch}$ in the real parts of Z-parameters [9], [15], but this parameter is kept in this paper to take into account the case of larger gate length. The accuracy of this calculation is sufficient because the effect of $R_{\rm ch}$ is negligible as the gate length becomes shorter. Short gate lengths (of about 0.2 μm) are usually small compared to the gate–source and gate–drain gaps (of about 0.9 μm). In addition, only a fraction of $R_{\rm ch}$ appears in series with the parasitic resistances R_g, R_s, R_d in the above Z-equations.

Moreover, when the transistor model is used for MMIC design, some approximations regarding the extrinsic resistances R_s and R_d can be made. Actually, a slight uncertainty on the determination of the values of R_s and R_d is acceptable, because it is directly compensated by another slight uncertainty on intrinsic resistances (R_j, R_i, or $1/G_d$). This argument is valid for HEMT's with different values of gatewidth, because all of the resistances of the equivalent circuit are inversely proportional to the gatewidth (except R_g).

The above-mentioned compensation is valid for the extrinsic resistance R_g, only if the gatewidth and the number of gate fingers are fixed. No extension to HEMT's with different gate-size parameters is allowed, because the R_g resistance is proportional to the gatewidth and inversely proportional to the square of the number of gate fingers.

Gate- and drain-pad capacitances are determined by linear regressions of $\mathrm{Im}(Y_{ij})$ for a gate voltage below pinchoff, which causes the depletion of the channel. Typically up to 5 GHz, the contribution of both series inductances and resistances are neglected. The corresponding equations are [1]

$$\mathrm{Im}(Y_{11}) = j\omega \cdot (C_{\rm pg} + 2 \cdot C_b) \tag{5a}$$

$$\mathrm{Im}(Y_{12}) = \mathrm{Im}(Y_{21}) = -j\omega \cdot C_b \tag{5b}$$

$$\mathrm{Im}(Y_{22}) = j\omega \cdot (C_{\rm pd} + C_b) \tag{5c}$$

where C_b is the resulting capacitance $C_{\rm gs}$ (equal to $C_{\rm gd}$, as the gate is centered in the drain–source gap, which is a necessary

approximation [7]) at these bias conditions. But the pads and intrinsic capacitances are not easily separated; in particular $C_{\rm pd}$ includes residual drain-to-source capacitance at pinchoff voltage. In reference [7], a physical method to separate the parasitic capacitances of the FET is presented, also including a dependence with the gatewidth.

In order to separate the two contributions, test patterns were fabricated, including only pads and interconnections (without the HEMT or its electrodes).

III. Determination of Intrinsic Parameters

A. Intrinsic Parameters Behavior

The determination of the intrinsic parameters is carried out using transformations of measured S-parameters into Z- and Y-parameters [1], for each bias point. The parasitic extrinsic parameters are de-embeded to obtain the intrinsic Y-parameters.

The Y-parameters expressions are calculated from the intrinsic equivalent circuit. A gate–drain resistance R_j is added to make the circuit symmetrical with regard to drain and source [3]. This is useful for an extension to large-signal modeling in the case of zero-volt drain-to-source voltage. In [14], [16], a $C_{\rm dc}$ capacitance is added between R_i and R_j, which physically results from a nonuniform free-charge density in the channel. The addition of R_j or $C_{\rm dc}$ causes $\mathrm{Re}(Y_{12})$ to vary as the square of the frequency, so R_j (chosen here) or $C_{\rm dc}$ have identical roles. While $\mathrm{Re}(Y_{12})$ is generally positive, $C_{\rm dc}$ usually has a positive value, and R_j a negative value. Adding R_j or $C_{\rm dc}$ leads the equivalent circuit to more closely fit the experimental S_{12}-parameter at HF, since the model described in [1] gives $\mathrm{Re}(Y_{12}) = 0$. Experimental results confirm this particular frequency behavior [3].

In addition, the accuracy of the short gate-length InP HEMT's equivalent circuit is improved by adding a frequency dependence of $C_{\rm ds}$, G_d, and G_m. The calculated intrinsic Y-parameters are

$$\begin{aligned}
Y_{11} &= \frac{R_i \cdot C_{\rm gs}^2 \cdot \omega^2}{D_1} + \frac{1}{R_{\rm gs}} + \frac{R_j \cdot C_{\rm gd}^2 \cdot \omega^2}{D_2} + \frac{1}{R_{\rm gd}} \\
&\quad + j\omega \cdot \left(\frac{C_{\rm gs}}{D_1} + \frac{C_{\rm gd}}{D_2} \right) \\
Y_{12} &= -\frac{R_j \cdot C_{\rm gd}^2 \cdot \omega^2}{D_2} - \frac{1}{R_{\rm gd}} - \frac{j\omega \cdot C_{\rm gd}}{D_2} \\
Y_{21} &= \frac{G_m(\omega) \cdot e^{-j\omega\tau}}{1 + j\omega \cdot R_i \cdot C_{\rm gs}} - \frac{R_j \cdot C_{\rm gd}^2 \cdot \omega^2}{D_2} \\
&\quad - \frac{1}{R_{\rm gd}} - \frac{j\omega \cdot C_{\rm gd}}{D_2} \\
Y_{22} &= G_d(\omega) + \frac{R_j \cdot C_{\rm gd}^2 \cdot \omega^2}{D_2} + \frac{1}{R_{\rm gd}} \\
&\quad + j\omega \cdot \left(C_{\rm ds}(\omega) + \frac{C_{\rm gd}}{D_2} \right) \qquad (6)
\end{aligned}$$

with

$$\begin{aligned}
D_1 &= 1 + R_i^2 \cdot C_{\rm gs}^2 \cdot \omega^2 \\
D_2 &= 1 + R_j^2 \cdot C_{\rm gd}^2 \cdot \omega^2.
\end{aligned}$$

A frequency dependence of extrinsic and, consequently, intrinsic parameters has already been used [15], [16], but a different approach is presented in this paper. In order to analytically describe the frequency dependence, each intrinsic parameter is systematically studied versus frequency. Both real and imaginary parts of measured Y_{ij}-parameters are plotted and compared with the graph of the empirical equations describing them. It appears that the intrinsic parameters R_j, $C_{\rm gd}$, $R_{\rm gd}$, R_i, $C_{\rm gs}$, $R_{\rm gs}$, τ are not frequency dependent. It is not the case for $C_{\rm ds}$, G_d, and G_m, which are frequency dependent beyond 20 GHz and can be closely described by the following equations:

$$\begin{aligned}
j\omega \cdot C_{\rm ds}(\omega) &= j \cdot \omega \cdot \mathbf{C_{ds_1}} + j \cdot C_{\rm ds_2} \cdot \omega^2 \\
G_d(\omega) &= \mathbf{G_{d_0}} + G_{d_1} \cdot \omega + G_{d_2} \cdot \omega^2 \\
G_m(\omega) &= \mathbf{G_{m_0}} + G_{m_1} \cdot \omega + G_{m_2} \cdot \omega^2. \qquad (7)
\end{aligned}$$

Several types of InP heterojunction field effect transistors (HFET's) and HEMT's of 0.2–0.8-μm gate length have been investigated to verify this set of analytical equations. The slope change according to frequency begins to clearly appear on the Y-parameter graphs beyond 20 GHz. Moreover, the frequency dependence of these intrinsic parameters is independent of extrinsic parameters variations around their nominal value. An experimental justification of these correcting coefficients is presented in Section V.

B. Intrinsic Parameter Extraction

The extraction of the equivalent circuit parameters from S-measured parameters uses the method of [1] to separate the real and imaginary parts of Y_{ij}-parameters. However, in this paper, the Y-parameters' equations are transformed to introduce functions depending on the angular frequency ω:

$$\mathrm{Im}(Y_{12}) = \frac{-C_{\rm gd} \cdot j\omega}{D_2} \qquad (8a)$$

$$\mathrm{Re}(Y_{12}) = -\frac{R_j \cdot C_{\rm gd}^2 \cdot \omega^2}{D_2} - \frac{1}{R_{\rm gd}} \qquad (8b)$$

$$\mathrm{Im}(Y_{11} + Y_{12}) = \frac{C_{\rm gs} \cdot j\omega}{D_1} \qquad (8c)$$

$$\mathrm{Re}(Y_{11} + Y_{12}) = \frac{R_i \cdot C_{\rm gs}^2 \cdot \omega^2}{D_1} + \frac{1}{R_{\rm gs}} \qquad (8d)$$

$$\mathrm{Im}(Y_{22} + Y_{12}) = j\omega \cdot C_{\rm ds}(\omega) \qquad (8e)$$

$$\mathrm{Re}(Y_{22} + Y_{12}) = G_d(\omega) \qquad (8f)$$

$$Y_{21} - Y_{12} = \frac{G_m(\omega) \cdot e^{-j\omega \cdot \tau}}{1 + j\omega \cdot R_i \cdot C_{\rm gs}}$$

is expressed in polar coordinates:

$$G_m(\omega) = \mathrm{magnitude}[(Y_{21} - Y_{12})(1 + j\omega \cdot R_i \cdot C_{\rm gs})] \qquad (8g)$$

$$\tau = \mathrm{phase}[(Y_{21} - Y_{12})(1 + j\omega \cdot R_i \cdot C_{\rm gs})] \qquad (8h)$$

where D_1 and D_2 have been defined in (6).

The left terms of (8a)–(8h) are then fitted by the corresponding function of the parameter ω, and the intrinsic parameters are successively calculated from the coefficients of

these functions. The extraction procedure of the coefficients is detailed in Section IV.

Another advantage of the authors' extraction method, compared to those giving analytical expressions of each intrinsic parameters [1], [3], [10], [14], or performing optimizations, is to be closer to the device microwave behavior described by the intrinsic Y-parameters, even if no direct physically based extraction as in [11], [13] has been made. Actually, an easy fitting of Y-parameters by appropriate functions gives the possibility of establishing and validating the authors' equivalent circuit graphically. Equivalent circuit intrinsic parameters are directly extracted from combined Y-parameters. The good agreement between Y-parameters values and their fitting function guarantees the validity of each intrinsic parameter extraction.

All intrinsic parameters of the equivalent circuit are similarly determined for all bias points. As the extraction method is fast (typically 2 min for 70 operating points on a PC 486/66 MHz) and accurate, it can be used directly after on-wafer measurements of short gate-length InP HEMT's.

IV. Extraction Methodology

The development of the extraction methodology is fundamental to solve (3a)–(3c), (5a)–(5c), and (8a)–(8h) described in the previous sections. The major difficulty consists of finding a convergent algorithm to solve the nonlinear system obtained from the least-squares method applied to rational functions. Easy implementation and efficient results are given by the following method, which is a new fruitful extension of the usual least-squares method.

Regressions have to be achieved on the following typical functions in order to extract the equivalent-circuit parameters from (3a) to (3c), (5a) to (5c), and (8a) to (8h):

$$f_1(\omega) = a + b\cdot\omega$$
for $R_s + R_{\rm ch}/2$ (3b)
$R_s + R_d + R_{\rm ch}$ (3c)

$$f_2(\omega) = b\cdot\omega$$
for L_s (3b), $L_s + L_d$ (3c)
C_b (5b)
$C_{\rm pd}$ (5c), $C_{\rm pg}$ (5a), and also τ (8h)

$$f_3(\omega) = a + b\cdot\omega + c\cdot\omega^2$$
for $G_d(\omega)$ (8f), and $G_m(\omega)$ (8g)

$$f_4(\omega) = b\cdot\omega + c\cdot\omega^2$$
for $C_{\rm ds}(\omega)$ (8e)

$$g_1(\omega) = a\cdot\omega + b\cdot\frac{\omega}{1 + x\cdot\omega^2}$$
for $L_g + L_s$ (3a)

$$g_2(\omega) = a + b\cdot\frac{1}{\omega^2}$$
used to get $R_g + R_s + R_{\rm ch}/3$ (3a)

$$g_3(\omega) = b\cdot\frac{\omega}{1 + x\cdot\omega^2}$$
for $C_{\rm gd}$ (8a), and also $C_{\rm gs}$ (8c)

$$g_4(\omega) = a + b\cdot\frac{\omega^2}{1 + x\cdot\omega^2}$$
for R_j and $R_{\rm gd}$ (8b)
and also R_i and $R_{\rm gs}$ (8d).

- Polynomial case: used for the $f_k(\omega) = a\cdot\alpha(\omega) + b\cdot\beta(\omega) + c\cdot\chi(\omega)$.
  According to the well-known least-squares method, the following system using a matrix formalism (shown at the bottom of the page) is solved to determine the unknowns a, b, and c, where $(\omega_i, y_i)_i$ is the set of points to be fitted by the functions f_k, and n is the absolute error function $(n = |\sum_i (y_i - f_k(\omega_i))^2|)$.
- Rational case: where x is the unknown involved in the rational $g_k(\omega) = a\cdot\alpha(\omega) + b\cdot\beta(\omega, x)$.
  The method consists of fixing the value of the unknown x, to again find the previous polynomial case, following these steps:
  1) normalizing ω_i and $g_k(\omega_i)$ according to the respective maximum values;
  2) making iterations starting from the initial minimal x_1 and maximal x_2 values of x as explained now. As x_1 and x_2 are fixed values, the above matrix solving procedure can be used for the two polynomial functions:

$$g_{k_p}(\omega) = a\cdot\alpha(\omega) + b\cdot\beta(\omega, \sqrt{x_1\cdot x_2}),$$
and
$$g_{k_q}(\omega) = a\cdot\alpha(\omega) + b\cdot\beta(\omega, \sqrt{(1+\varepsilon)\cdot x_1\cdot x_2}).$$

The optimized values of a and b are obtained for each equation. The least-square relative error is then calculated by:

$$\text{Error} = \frac{\left|\sum_i (y_i - g_k(\omega_i))^2\right|}{\sum_i y_i}.$$

If $\text{Error}(g_{k_p}) < \text{Error}(g_{k_q})$, then x_2 is taken to be equal to $\sqrt{x_1\cdot x_2}$, while x_1 keeps its value (otherwise x_1 is taken to be equal to $\sqrt{x_1\cdot x_2}$, while x_2 keeps its value). This is equivalent to a dichotomy with a logarithmic scale.

When x_1 and x_2 are equal within approximately 5%, then the corresponding a, b, and $x = x_1 \cong x_2$ values are

$$\frac{1}{2}\cdot\begin{pmatrix}\frac{\partial n}{\partial a}\\ \frac{\partial n}{\partial b}\\ \frac{\partial n}{\partial c}\end{pmatrix} = \begin{pmatrix}\sum_i \alpha^2(\omega_i) & \sum_i \alpha(\omega_i)\cdot\beta(\omega_i) & \sum_i \alpha(\omega_i)\cdot\chi(\omega_i)\\ \sum_i \alpha(\omega_i)\cdot\beta(\omega_i) & \sum_i \beta^2(\omega_i) & \sum_i \beta(\omega_i)\cdot\chi(\omega_i)\\ \sum_i \alpha(\omega_i)\cdot\chi(\omega_i) & \sum_i \beta(\omega_i)\cdot\chi(\omega_i) & \sum_i \chi^2(\omega_i)\end{pmatrix}\cdot\begin{pmatrix}a\\ b\\ c\end{pmatrix} - \begin{pmatrix}\sum_i y_i\cdot\alpha(\omega_i)\\ \sum_i y_i\cdot\beta(\omega_i)\\ \sum_i y_i\cdot\chi(\omega_i)\end{pmatrix} = \begin{pmatrix}0\\0\\0\end{pmatrix}$$

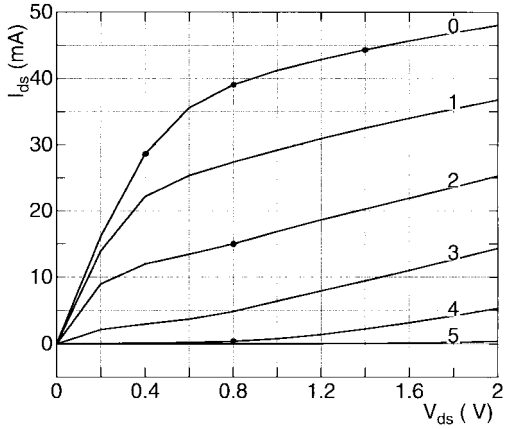

(a)

Extrinsic parameters :	Intrinsic parameters :
Cpg=5.3fF Cpd=25fF (Cb=39.3fF)	Cgd=37.6fF Rgd=-11.5Ω Cgs=97.3fF Ri=12.8Ω
Ls=10.7pH Lg=11.9pH Ld=39.2pH	Cds1=58.1fF Cds2=-1.65E-25 S/Hz² Gd0=24.9mS
Rs=4.1Ω Rg=2.7Ω Rd=4.3Ω (Rc=0.5Ω) (Ch=154fF/Rh=10.9kΩ)	Gd1=15.5E-15 S/Hz Gd2=-2.45E-26 S/Hz² Gm0=93.3mS Gm1=8.51E-14 S/Hz Gm2=-1.09E-25 S/Hz²
	Ft=91.7GHz

(b)

Fig. 4. (a) $I_{\rm ds}(V_{\rm ds}, V_{\rm gs})$ static characteristics of the 0.25 × 100-μm^2 InP HEMT used as example in Figs. 2–9. (0: $V_{\rm gs} = 0$ V), (1: $V_{\rm gs} = -0.2$ V), (2: $V_{\rm gs} = -0.4$ V), (3: $V_{\rm gs} = -0.6$ V), (4: $V_{\rm gs} = -0.8$ V), (5: $V_{\rm gs} = -1$ V). The points indicate the representative operating points chosen in Fig. 9. (b) Table showing extrinsic and intrinsic parameters extracted at the operating point $V_{\rm gs} = 0$V/$V_{\rm ds} = 0.8$ V.

the solutions, and are then denormalized; otherwise one goes to b) for a new iteration loop.

This method can be easily extended to similar functions with any order of ω. It is almost instantaneous, and gives an excellent fit.

V. Experimental Results

Different types of InP HFET's and HEMT's of 0.2–0.8-μm gate length fabricated in the authors' laboratory have been investigated to verify the authors' model, and to compare it with previously published results. Figures are now presented for the same 0.25 × 100 μm^2 InP HEMT. The static and microwave measurements, and the InP HEMT's extraction are implemented in a single software. A small-signal simulator uses uncompiled models with frequency-dependent elements.

Fig. 4 presents the static characteristics and the extrinsic and intrinsic parameters extracted at the onset of saturation, for a 0.25 μm InP HEMT. Figs. 5–7 show the frequency behavior of $C_{\rm ds}$, G_m, and G_d as follows:

- As shown in Fig. 5, a parabolic behavior with frequency clearly appears on $\mathrm{Im}(Y_{22} + Y_{12}) = j\omega \cdot C_{\rm ds}(\omega)$ (8e).

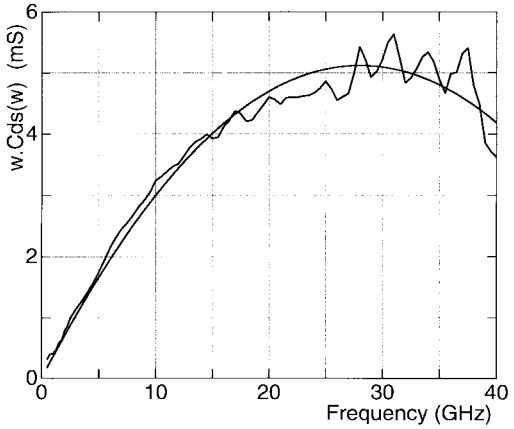

Fig. 5. Evolution of $j(\omega)\cdot C_{ds}(\omega) = \mathrm{Im}(Y_{22}+Y_{12})$ (8e) versus frequency. (0.25 × 100-μm^2 InP HEMT) $V_{\rm gs} = 0$ V/$V_{\rm ds} = 0.8$ V.

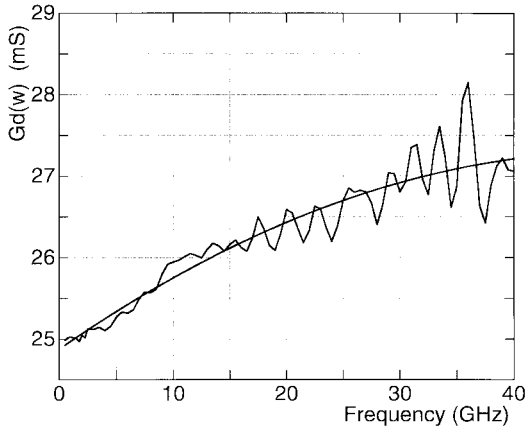

Fig. 6. Evolution of $G_d(\omega) = \mathrm{Re}(Y_{22} + Y_{12})$ (8f) versus frequency. G_d increases at about 8.8% at 40 GHz as compared to 1 GHz, at $V_{\rm gs} = 0$ V/$V_{\rm ds} = 0.8$ V.

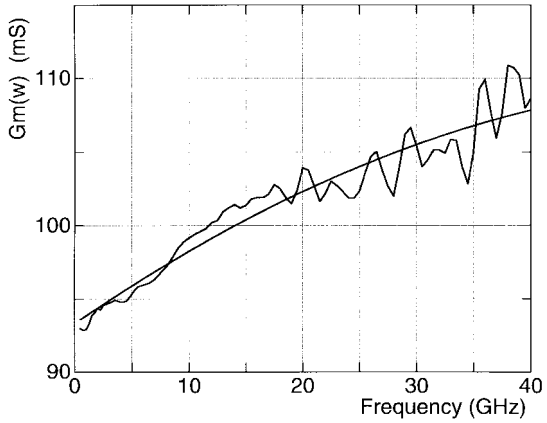

Fig. 7. Evolution of $G_m(\omega)$ described by (8g). G_m increases at about 14.9% at 40 GHz as compared to 1 GHz, at $V_{\rm gs} = 0$ V/$V_{\rm ds} = 0.8$V.

This effect already exists on $\mathrm{Im}(Y_{22})$ even with good extrinsic capacitance values, though an overevaluation of the pad capacitance $C_{\rm pd}$ (already solved in Section II) causes the parabolic behavior of $\mathrm{Im}(Y_{22})$ to increase. The parabolic behavior of $\mathrm{Im}(Y_{22} + Y_{12})$ is more obvious because $\mathrm{Im}(Y_{12})$ (8a) is equivalent to $\frac{-1}{R_j^2 \cdot C_{\rm gd} \cdot \omega}$ at HF (for $\omega \gg \frac{1}{R_j \cdot C_{\rm gd}}$).

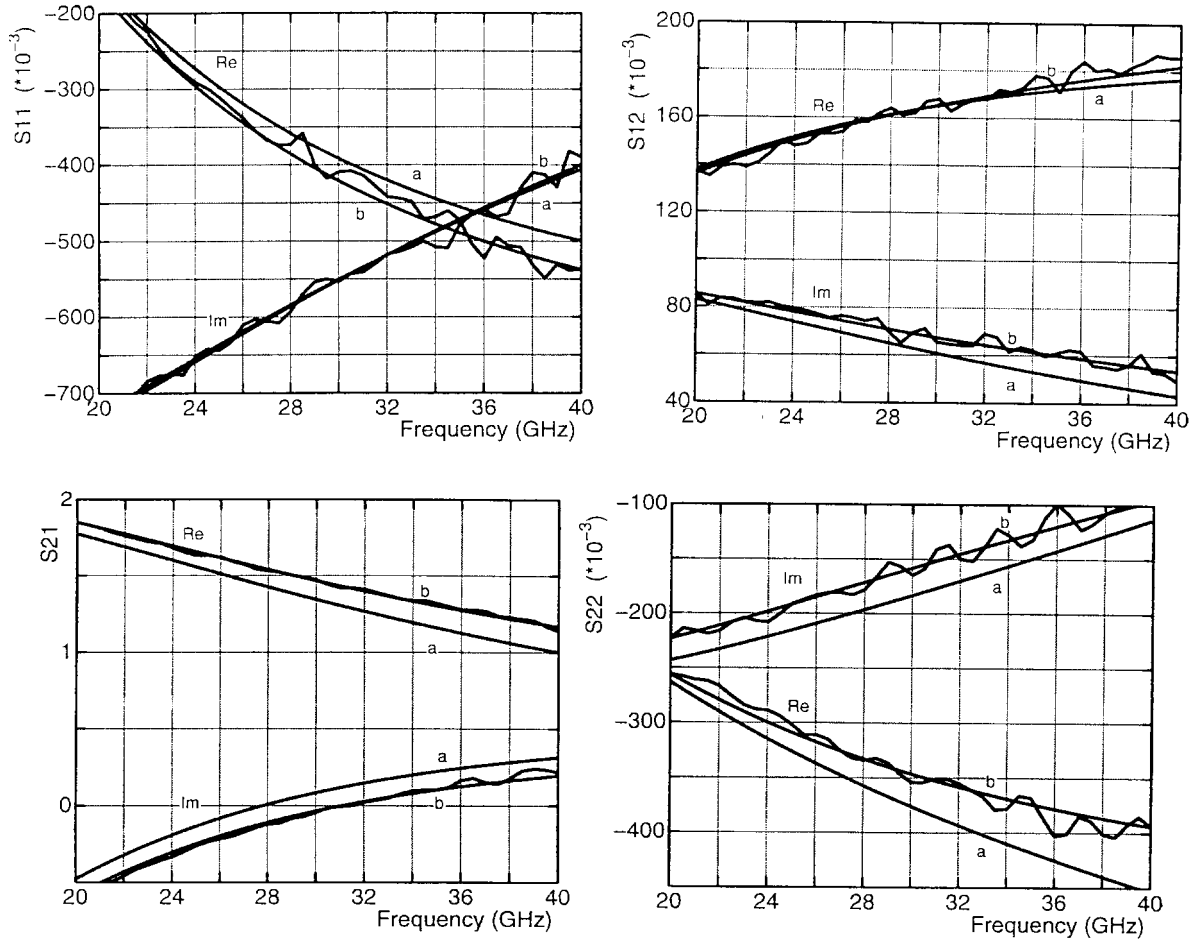

Δ_{ab}(40GHz)	S11	S12	S21	S22
Re	6.0%	3.5%	16.5%	11.0%
Im	1.5%	9.0%	10.0%	5.5%

Fig. 8. Comparison of measured S-parameters (jagged lines) (0.25 × 100-μm^2 InP HEMT) with simulation results of the method proposed in [3]: a-curves, and the authors' procedure: b-curves, at $V_{\rm gs} = 0$ V/$V_{\rm ds} = 0.8$ V ·Δ_{ab} represents the relative differences between a-curves and b-curves S-parameters (normalized with $|S_{ij}|$ at 40 GHz.

- As shown in Figs. 6 and 7, $\mathrm{Re}(Y_{22}+Y_{12}) = G_d(\omega)$ (8f) and $G_m(\omega)$ (8g) exhibit a parabolic behavior beyond 20 GHz.
- $C_{\rm ds}$, G_d, and G_m sufficiently move versus frequency, so that, at HF, those effects described by (7) cannot be neglected.

Measured S-parameters are compared with simulation results of the method proposed in [3] with the authors' procedure using frequency polynomial dependence of $C_{\rm ds}$, G_d, and G_m. The results are shown in Fig. 8. The authors' model yields better accuracy at HF, basically resulting from the very good agreement between the real and imaginary parts of Y-parameters, with (6) and (7) calculated from the equivalent circuit, up to 40 GHz.

Final results are presented as real/imaginary parts for typical operating points chosen on the $I_{\rm ds}(V_{\rm ds})$ characteristics, on Fig. 9. In spite of a slight uncertainty on a simulated S_{11}-parameter above 25 GHz in the pinchoff region, there is very good agreement between measured and simulated S-parameters for all operating points over a 500-MHz to 40-GHz frequency range.

However, a major limitation concerning equivalent circuits is the ability to extrapolate them beyond the measurement range. In particular, many of the 100-GHz HEMT devices being designed up until now are designed using equivalent circuits from 0 to 40–60-GHz measurements and extrapolating constant parameters. Polynomials offer a good extrapolation outside the frequency range as long as the higher order terms remain small, in order to keep their corrective effect. An estimation of the extrapolation validity was recently confirmed with measurements in the 80-GHz frequency range.

VI. Conclusion

A small-signal equivalent circuit for short gate-length InP HEMT's at very HF is presented. The cold-HEMT modeling without forward biasing the gate is described. A frequency

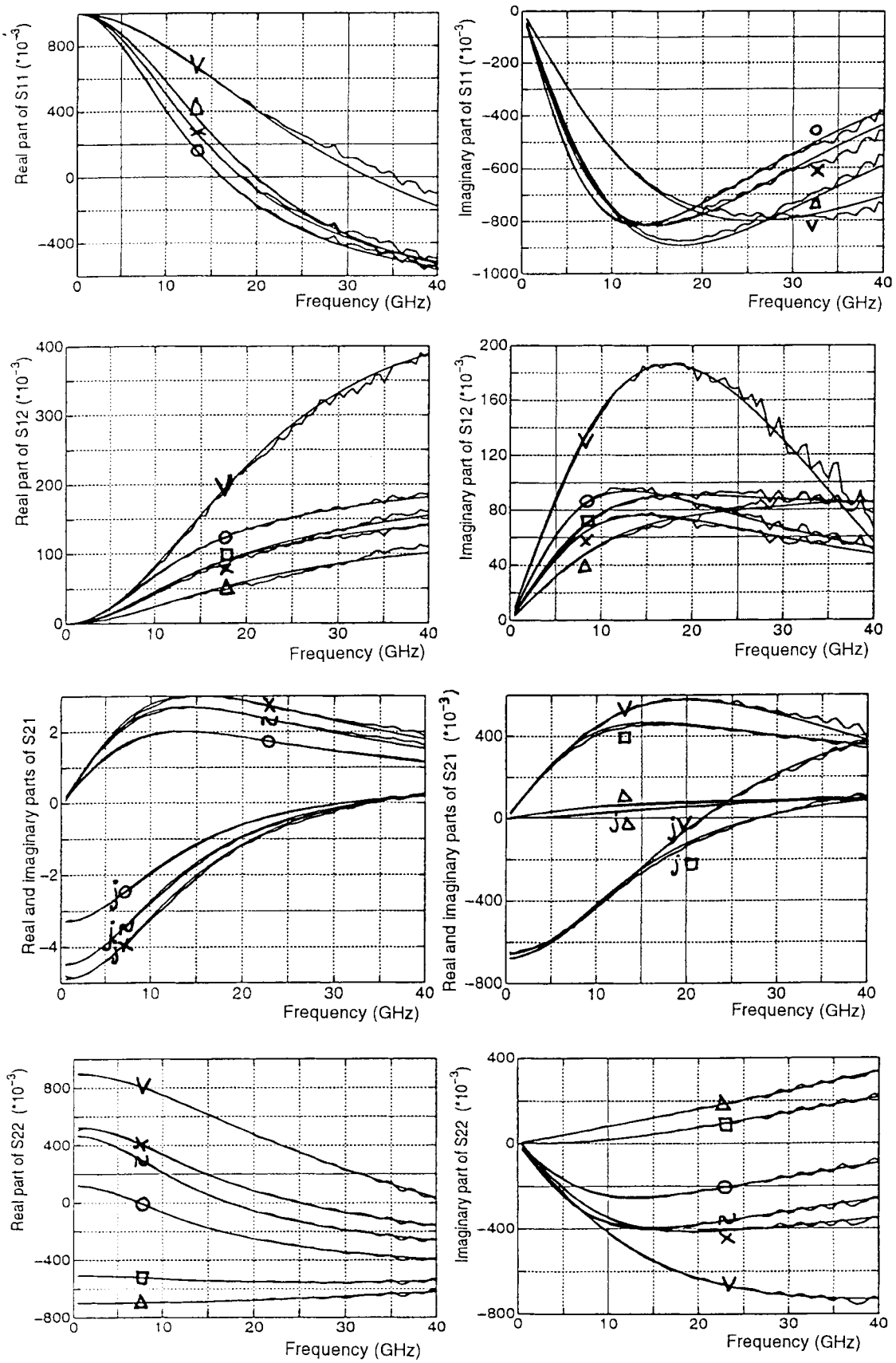

Fig. 9. Real and imaginary parts of the measured (jagged lines) and simulated (smooth lines) S-parameters up to 40 GHz (0.25 $\times$ 100 μm^2 InP HEMT) for representative operating points [see Fig. 4(a)]: Δ : $V_{\rm gs} = 0$ V/$V_{\rm ds} = 0$ V (cold model), r : $V_{\rm gs} = 0$ V/$V_{\rm ds} = 0.4$ V (ohmic region), O : $V_{\rm gs} = 0$ V/$V_{\rm ds} = 0.8$ V (at the boundary between ohmic and saturation region), $*$: $V_{\rm gs} = 0$ V/$V_{\rm ds} = 1.4$ V (saturation region), ˜: $V_{\rm gs} = -0.4$ V/$V_{\rm ds} = 0.8$ V. V : $V_{\rm gs} = -0.8$ V/$V_{\rm ds} = 0.8$ V (pinchoff region). For S_{21}-paramaters, the real and imaginary parts are presented on two graphs which have two different scales. For S_{11}- and S_{12}-parameters, one or two bias points are removed for a better readability.

polynomial dependence of some intrinsic parameters over the 15–40-GHz frequency range is taken into account and leads to a more accurate model. The described new and fast method to determine the equivalent circuit elements is closely involved in both establishment of the empirical equations and accurate extraction solving. It is well adapted for on-wafer characterization. Plotting the real and imaginary parts of Y-parameters, and their fit by the equations describing the equivalent circuit, is an effective way to verify and validate the model. Very good agreement between measured and simulated S-parameters over a 500-MHz to 40-GHz frequency range has been demonstrated for typical bias points.

ACKNOWLEDGMENT

The authors would like to thank R. Lefèvre and A. Scavennec for their interest and support, and A. Clei and R. Palla for design and fabrication of InP HEMT's and for measurement of the S-parameters.

REFERENCES

[1] G. Dambrine, A. Cappy, F. Héliodore, and E. Playez, "A new method for determining the FET small-signal equivalent circuit," *IEEE Trans. Microwave Theory Tech.*, vol. 36, pp. 1151–1159, July 1988.
[2] M. Berroth and R. Bosch, "Broad-band determination of the FET small-signal equivalent circuit," *IEEE Trans. Microwave Theory Tech.*, vol. 38, pp. 891–895, July 1990.
[3] ——, "High-frequency equivalent circuit of GaAs FET's for large-signal applications," *IEEE Trans. Microwave Theory Tech.*, vol. 39, pp. 224–229, Feb. 1991.
[4] P. L. Hower and N. G. Bechtel, "Current saturation and small-signal characteristics of GaAs field-effect transistors," *IEEE Trans. Electron Devices*, vol. ED-20, pp. 213–220, Mar. 1973.
[5] H. Fukui, "Determination of the basic device parameters of the GaAs MESFET," *Bell Syst. Tech. J.*, vol. 58, pp. 771–797, Mar. 1979.
[6] R. Anholt and S. Swirhun, "Equivalent-circuit parameter extraction for cold GaAs MESFET's," *IEEE Trans. Microwave Theory Tech.*, vol. 39, pp. 1243–1246, July 1991.
[7] ——, "Measurement and analysis of GaAs MESFET parasitic capacitances," *IEEE Trans. Microwave Theory Tech.*, vol. 39, pp. 1247–1251, July 1991.
[8] E. Arnold, M. Golio, M. Miller, and B. Beckwith, "Direct extraction of GaAs MESFET intrinsic element and parasitic inductance values," in *IEEE MTT-S Dig.*, I-24, 1990, pp. 359–362.
[9] I. Corbella, J. M. Legido, and G. Naval, "Instantaneous model of a MESFET for use in linear and non linear circuit simulations," *IEEE Trans. Microwave Theory Tech.*, vol. 40, pp. 1410–1421, July 1992.
[10] K. Nagatomo, Y. Daido, M. Shimizu, and N. Okubo, "GaAs MESFET characterization using least squares approximation by rational functions," *IEEE Trans. Microwave Theory Tech.*, vol. 41, pp. 199–205, Feb. 1993.
[11] S. J. Mahon, D. J. Skellern, and F. Green, "A technique for modeling S-parameters for HEMT structures as a function of gate bias," *IEEE Trans. Microwave Theory Tech.*, vol. 40, pp. 1430–1440, July 1992.
[12] S. J. Mahon, M. J. Chivers, and D. J. Skellern, "Simulation of HEMT dc drain current and 1 to 50 GHz S-parameters as a function of gate bias," *IEEE Trans. Microwave Theory Tech.*, vol. 41, pp. 1065–1067, June/July 1993.
[13] S. J. Mahon and D. J. Skellern, "Modeling drain and gate dependence of HEMT 1–50 GHz, small-signal S-parameters, and dc drain current," *IEEE Trans. Microwave Theory Tech.*, vol. 43, pp. 213–216, Jan. 1995.
[14] H. O. Vickes, "Determination of intrinsic FET parameters using circuit partitioning approach," *IEEE Trans. Microwave Theory Tech.*, vol. 39, pp. 363–366, Feb. 1991.
[15] A. Eskandarian and S. Weinreb, "A note on experimental determination of small-signal equivalent circuit of millimeter-wave FET's," *IEEE Trans. Microwave Theory Tech.*, vol. 41, pp. 159–162, Jan. 1993.
[16] R. T. Webster, A. J. Slobodnik, and G. A. Roberts, "Determination of InP HEMT noise parameters and S-parameters to 60 GHz," *IEEE Trans. Microwave Theory Tech.*, vol. 43, pp. 1216–1225, June 1995.

Agnès Miras was born in Alès, France, on May 27, 1970. She received the Dipl. Eng. degree from Ecole Centrale de Lille, France, in 1994. Her third year of engineering studies was spent at Ecole Centrale de Paris, Paris, France, with a specialization in electronics.

She joined the Laboratoire de Bagneux, France-Télécom CNET, Bagneux Cedex, France, in 1994, where she is working toward the Ph.D. degree in micro- and opto-electronics at the University of Orsay Paris XI, Paris, France. She is involved in both the development of CAO models for InP HEMT's, and high-speed telecommunication MMIC design based on GaAs or InP technology for photoreception applications.

Eric Legros was born in Fontainebleau, France, on November 7, 1966. He received the Dipl. Eng. degree from Ecole Polytechnique, France, in 1989, and the Ph.D. degree in microelectronics from the University of Paris XI Orsay, France, in 1993, where his work has focused on low-noise-preamplifier design for coherent and direct detection.

In 1994, he joined the team involved in III–V components and circuits for optical communications at the Laboratoire de Bagneux, France-Télécom CNET, Bagneux Cedex, France. His main research activity is the design of MMIC and optoelectronic modules for both distribution and high-speed telecommunication systems.